Numerical Simulation of Surfactant Flooding and Its Application in Low Permeability Reservoir

Yin Daiyin and Zhou Yazhou

Institute of Petroleum Engineering, Northeast Petroleum University, China

yindaiyin@163.com, zhouyazhou720@163.com

Abstract

With the development of computer science, the numerical simulation of oil reservoirs has been advanced and widely applied. In this paper, according to the surfactant flooding mechanism, a mathematical model for three dimension two-phase three-component surfactant flooding is established. The numerical difference equation is solved using implicit method for pressure and concentration terms and explicit method for saturation terms. A new method is used to treat the relation between the adsorption of the surfactant and the relative permeability curve, which reduces the discrepancy between the mathematical model and the data from actual production. The model is programmed into software using FOR90 language. The software is used to study the surfactant displacement in Chao 61 district of Daqing oilfield. An optimization is done for the injection plan of the surfactant. The oilfield experiment shows that the optimal scheme reduces the threshold pressure of low permeability reservoirs and increases the water absorption rate. The reservoir production ratio increases as well.

Keywords: *surfactant flooding, numerical simulation, low permeability reservoir, mathematical model*

1. Introduction

Recently, with the continuing development of computer science, applied mathematics, and reservoir engineering, the numerical simulation for oil reservoirs has been rapidly advanced and widely applied. The motion of the fluid, the oil displacement mechanism, and the space distribution of the residual oil can be revealed by the numerical simulation [1-3]. Based on these pieces of information, the best mining parameters and the most rational development plan can be selected, leading to minimum investment and maximum recovery and economic benefits.

For the past twenty years, most of the large oilfields in the world have stepped into a late development stage where water injections were used, facing more difficulties in the production of the remaining oil [4-6]. Chemical flooding enhanced oil recovery (EOR) has gradually become a focus to the researchers. A series of laboratory and Oilfield experiments were carried out for polymer flooding, alkaline-polymer flooding, surfactant-polymer flooding, and alkaline-surfactant-polymer flooding and a number of achievements were accomplished. However, these studies mostly focused on reservoirs with medium to high permeability. Commercial software for polymer flooding simulations such as 'POLYMER' and 'VIP-POLYMER' are published [7-8]. There are two types of numerical simulations or simulation software that can be found in the literature for alkaline-surfactant-polymer flooding. The first is a black oil model based alkaline flooding model. In this model, changes in the phase viscosity, relative permeability, and fluid behavior caused by the addition of alkali are considered using a simplified approach. The mechanisms and physical and chemical phenomena in the flooding process are not detailed in the model. Therefore, this kind of models only suits for preliminary simulations. The basic

assumptions made in these models are constant temperature, negligible diffusion of chemicals, and negligible impact from the change in salt composition. The other type is compound flooding component model. The model based on mass balance equations for all the components. Therefore, the effects of the change in the concentrations in each component on all kinds of physical and chemical phenomena can be analyzed. Currently, the University of Texas takes the leading role in the study of chemical compound flooding component model. Byuyanhe and Pope *et al.*, have added the alkali flooding function to the micelle-polymer flooding model, which is called the UTCHEM model. The basic assumptions made in this model are: thermal equilibrium for all points in the reservoir, constant temperature, lumping all the acidic components to one, HA, which is highly dissolvable in oil and a distribution constant can be assigned to it for its separation in oil and water phase, negligible temperature, pressure, and volume change from chemical reaction, and slightly compressible fluid in the reservoir. There are several shortcomings of UTCHEM [9-11]. First, due to that a large number of factors are taken into account in the model, an equation system with a huge size needs to be solved. If the implicit method in pressure terms and the explicit method in saturation and concentration terms are used to solve the equation, the accuracy and convergence of the computation will be affected. Additionally, the software only deals with two-dimensional problems, which ignores the variations in the thickness of the oil reservoir. Finally, the dead nodes (where the permeability, the porosity, or the effective oil layer thickness is zero) are not allowed in the model. Such software only considers little geological conditions of the reservoir, which leads to errors in simulation results. As a result, the software is only used for studies on mechanisms. Little focus has been put on the indoor and oilfield experiments and numerical simulations for surfactant flooding in low permeability oil reservoirs.

2. The Setup of the Surfactant Flooding Model

2.1. Basic assumptions

1) Two-phase (oil-water) flow system in the reservoir;

2) Three components: oil, water, and surfactant;

3) The rocks and the fluid are compressible;

4) The rocks are anisotropic and the density is non-uniformly distributed;

5) Convectional diffusion is considered;

6) The adsorption to rocks is considered;

7) The capillary pressure is considered;

8) The gravitational force is considered.

2.2. Setup of the model

In the process of surfactant water solution flooding, the diffusion from the water solution to the oil phase and the adsorption to the surface of the reservoir sandstone solid particles of the surfactant take place at the same time. Also, physical and chemical phenomena such as changes in rheological properties of crude oil and capillary pressure exist.

These phenomena complicate the surfactant flooding condition by changing the quantitative relations that determine the flooding mechanism. Therefore, the evaluation of the effectiveness of the methods is also affected. As a result, a mathematical model that describes the surfactant flooding process need to be established.

The model is a PDE system for multi-component multi-phase isothermal flow system. First of all, the non-equilibrium flow is considered for the n components in the m phases when temperature is constant. Taking into account the diffusion and the adsorption to the surface of porous media for each component, the continuous equation for the j^{th} component in the i^{th} phase can be written as:

$$\nabla \cdot [\phi D_{ij} s_i \nabla(\rho_j C_{ij})] - \nabla \cdot (\rho_j \mathbf{V_i} C_{ij}) - \sum_{a=1}^{m} \eta_{aij}(\varphi_{ij} - \varphi_{aj}) = \frac{\partial}{\partial t}(\phi \rho_j s_i C_{ij} + \rho_j a_{ij}) - \rho_j q_i C_{ij} \quad (1)$$

The saturation and the mass fraction for each phase and component are related by:

$$\sum_{i=1}^{m} s_i = 1 \ , \ \sum_{j=1}^{n} C_{ij} = 1 , \ i = 1,\ldots, m \quad (2)$$

The flow rate in the i^{th} phase is expressed by the non-Darcy equation:

$$\mathbf{V_i} = -\frac{KK_{ri}}{\mu_i}(\nabla p_i - \rho_i g \nabla z \pm \mathrm{D_p}) \quad (3)$$

The pressure in each phase is related by:

$$p_{cai} = p_a - p_i \ , \ i=1,\ldots, n \quad (4)$$

Generally, the capillary pressure p_{cai} is a function of saturation and phase composition.

In order to close the equation system, besides the viscosity in each phase, density, relative permeability, capillary pressure, absolute permeability tensor, porosity, and convectional diffusion tensor, the transfer between phases for each component should also be specified. At the interface of phases, equilibrium has been reached for each component locally. Diffusion happens between the interface and the nearby continuous phase for each component. The ability to separate from its original phase for any component depends on its chemical potential. Spontaneous transfer takes place from the phase with high component chemical potential to the phase with low component chemical potential until equilibrium is reached. According to the characteristics of productions of oilfields, the velocity of the fluid in the pores of the reservoirs is small. Therefore, it is reasonable to assume that the transfer between phases is always at equilibrium under the formation conditions, i.e. for a sufficient long time in the porous media, the time needed for the chemical potentials to equilibrate is much shorter than the time needed for the saturations of the phases to have considerable changes. For example, for a practical flow velocity, the process where CO_2 transfers from water phase to oil phase equilibrates within a model with several meters. As a result, in the study of multi-component flow, it can be assumed that local thermal dynamic equilibrium is established at each point in the reservoir. According to the above, the chemical driving force term can be neglected to simplify the surfactant flooding model and reduce the number of experiments that are needed to determine the parameters in the computation.

According to Equation (3) and summing Equation (1) over *i*, the continuous equation for the j^{th} component can be obtained as:

$$\nabla \cdot \sum_{i=1}^{m} \left[\phi D_{ij} s_i \nabla(\rho_j C_{ij}) + \frac{KK_{ri}\rho_i}{\mu_i} \varepsilon_i C_{ij} (\nabla p_i - \rho_i g \nabla z \pm \mathrm{D_p}) \right] = \frac{\partial}{\partial t} \sum_{i=1}^{m} (\phi \rho_j s_i C_{ij} + \rho_j a_{ij}) - \sum_{i=1}^{m} \rho_j q_i C_{ij} \quad (5)$$

The composition variations during the surfactant solution flooding process are analyzed below. According to the multi-component mixture simulation principles, the components that

cannot be decomposed are selected first. For the surfactant flooding, only two phases exist: oil phase and water phase. Then, the three components, namely oil, water, and surfactant, are defined in each phase. Thus, the process can be described by a two-phase three-component flow equation system where *i* is either oil or water (o or w) and *j*=1, 2, and 3 which stand for oil, water, and surfactant, respectively. The direction of z axis is chosen to be straight downwards.

$$\mathbf{V}_{\mathrm{o}} = -\frac{kk_{\mathrm{ro}}}{\mu_{\mathrm{o}}}\left(\frac{dp}{dx} \pm \mathrm{D}_{\mathrm{p}}(\mathrm{C}, s_{\mathrm{w}})\right) \tag{6}$$

$$\mathbf{V}_{\mathrm{w}} = -\frac{kk_{\mathrm{rw}}}{\mu_{\mathrm{w}}}\left(\frac{dp}{dx} \pm \mathrm{D}_{\mathrm{p}}(\mathrm{C}, s_{\mathrm{w}})\right) \tag{7}$$

In the above equations, if $\frac{dp}{dx} \geq 0$, then the threshold pressure gradient takes positive sign and negative sign, otherwise, if $\frac{dp}{dx} - \mathrm{D}_{\mathrm{p}}(\mathrm{C}, s_{\mathrm{w}}) \leq 0$, then $\mathbf{V}_{\mathrm{o}} = 0$, $\mathbf{V}_{\mathrm{w}} = 0$.

Under the above conditions, D_{ij} and a_{ij} for components oil and water can be neglected. The resulting equation system with conventional signs can be written as:

$$\nabla \cdot [\frac{KK_{\mathrm{ro}}\rho_{\mathrm{o}}}{\mu_{\mathrm{o}}} C_{\mathrm{o1}}(\nabla p_{\mathrm{o}} - \rho_{\mathrm{o}} g \nabla \mathrm{z} \pm \mathrm{D}_{\mathrm{p}}) + \frac{KK_{\mathrm{w}}\rho_{\mathrm{w}}}{\mu_{\mathrm{w}}} C_{\mathrm{w1}}(\nabla p_{\mathrm{w}} - \rho_{\mathrm{w}} g \nabla \mathrm{z} \pm \mathrm{D}_{\mathrm{p}})] = \frac{\partial}{\partial t}\phi(\rho_{\mathrm{o}} s_{\mathrm{o}} C_{\mathrm{o1}} + \rho_{\mathrm{w}} s_{\mathrm{w}} C_{\mathrm{w1}}) - \rho_{\mathrm{o}} q_{\mathrm{o}} C_{\mathrm{o1}} - \rho_{\mathrm{w}} q_{\mathrm{w}} C_{\mathrm{w1}} \tag{8}$$

$$\nabla \cdot [\frac{KK_{\mathrm{ro}}\rho_{\mathrm{o}}}{\mu_{\mathrm{o}}} C_{\mathrm{o2}}(\nabla p_{\mathrm{o}} - \rho_{\mathrm{o}} g \nabla \mathrm{z} \pm \mathrm{D}_{\mathrm{p}}) + \frac{KK_{\mathrm{rw}}\rho_{\mathrm{w}}}{\mu_{\mathrm{w}}} C_{\mathrm{w2}}(\nabla p_{\mathrm{w}} - \rho_{\mathrm{w}} g \nabla \mathrm{z} \pm \mathrm{D}_{\mathrm{p}})] = \frac{\partial}{\partial t}\phi(\rho_{\mathrm{o}} s_{\mathrm{o}} C_{\mathrm{o2}} + \rho_{\mathrm{w}} s_{\mathrm{w}} C_{\mathrm{w2}}) - \rho_{\mathrm{o}} q_{\mathrm{o}} C_{\mathrm{o2}} - \rho_{\mathrm{w}} q_{\mathrm{w}} C_{\mathrm{w2}} \tag{9}$$

$$\nabla \cdot \varphi[D_{\mathrm{o3}} s_{\mathrm{o}} \nabla(\rho_3 C_{\mathrm{o3}}) + D_{\mathrm{w3}} s_{\mathrm{w}} \nabla(\rho_3 C_{\mathrm{w3}})] + \nabla \cdot K[\frac{K_{\mathrm{ro}}\rho_3}{\mu_{\mathrm{o}}} C_{\mathrm{o3}}(\nabla p_{\mathrm{o}} - \rho_{\mathrm{o}} g \nabla \mathrm{z} \pm \mathrm{D}_{\mathrm{p}}) + \frac{K_{\mathrm{rw}}\rho_3}{\mu_{\mathrm{w}}} C_{\mathrm{w3}}$$
$$(\nabla p_{\mathrm{w}} - \rho_{\mathrm{w}} g \nabla \mathrm{z} \pm \mathrm{D}_{\mathrm{p}})] = \frac{\partial}{\partial t}(\varphi\rho_3 s_{\mathrm{o}} C_{\mathrm{o3}} + \rho_3 a_{\mathrm{o3}} + \varphi\rho_3 s_{\mathrm{w}} C_{\mathrm{w3}} + \rho_3 a_{\mathrm{w3}}) - \rho_3 q_{\mathrm{o}} C_{\mathrm{o3}} - \rho_3 q_{\mathrm{w}} C_{\mathrm{w3}} \tag{10}$$

$$p_{\mathrm{c}} = p_{\mathrm{o}} - p_{\mathrm{w}} \tag{11}$$

$$s_{\mathrm{o}} + s_{\mathrm{w}} = 1 \tag{12}$$

$$C_{\mathrm{o1}} + C_{\mathrm{o3}} = 1 \tag{13}$$

$$C_{\mathrm{w2}} + C_{\mathrm{w3}} = 1 \tag{14}$$

There are eight unknowns in seven equations from Equation (11) to (14), which are p_{o}, p_{w}, s_{o}, s_{w}, C_{o1}, C_{w2}, C_{o3}, and C_{w3}. The phase equilibrium condition should be added in order to have a solution from the equation system.

$$M = C_{\mathrm{o3}} / C_{\mathrm{w3}} \tag{15}$$

3. Solution Method for the Surfactant Flooding Model

3.1. The basic idea

1) Using implicit methods for pressure and concentration and explicit method for saturation to solve the equation system;

2) Pressures are computed using an implicit method with the coefficients evaluated at time *n*;

3) Pressures are plugged in Equation (11) and (12) for saturations;

4) The pressure P_o and saturation S_w are substituted into Equation (10) and (15) to compute C_{o3} and C_{w3} implicitly.

3.2. The difference equations for pressure

Using the block center gird, Equation (8) after discretization becomes:

$$a_{i,j,k-1}p_{o,i,j,k-1}^{n+1}+b_{i,j-1,k}p_{o,i,j-1,k}^{n+1}+c_{i-1,j,k}p_{o,i-1,j,k}^{n+1}+d_{i,j,k}p_{o,i,j,k}^{n+1}+e_{i,j,k+1}p_{o,i,j,k+1}^{n+1}+ f_{i,j+1,k}p_{o,i,j+1,k}^{n+1}+g_{i+1,j,k}p_{o,i+1,j,k}^{n+1}=H_{i,j,k}^{n+1} \tag{16}$$

The sign of the threshold pressure gradient should depend on the sign of $\frac{dp^n}{dx}$, which always makes the threshold pressure gradient a resistance.

Where: $a_{i,j,k-1}=\frac{T^n_{ozk-\frac{1}{2}}}{T^n_{o\phi}}+\frac{T^n_{wzk-\frac{1}{2}}}{T^n_{w\phi}}$, $b_{i,j-1,k}=\frac{T^n_{oyj-\frac{1}{2}}}{T^n_{o\phi}}+\frac{T^n_{wyj-\frac{1}{2}}}{T^n_{w\phi}}$, $c_{i-1,j,k}=\frac{T^n_{oxi-\frac{1}{2}}}{T^n_{o\phi}}+\frac{T^n_{wxi-\frac{1}{2}}}{T^n_{w\phi}}$,

$$d_{i,j,k}=\frac{T^n_{ozk-\frac{1}{2}}}{T^n_{o\varphi}}+\frac{T^n_{wzk-\frac{1}{2}}}{T^n_{w\varphi}}+\frac{T^n_{oyj-\frac{1}{2}}}{T^n_{o\varphi}}+\frac{T^n_{wyj-\frac{1}{2}}}{T^n_{w\varphi}}+\frac{T^n_{oxi-\frac{1}{2}}}{T^n_{o\varphi}}+\frac{T^n_{wxi-\frac{1}{2}}}{T^n_{w\varphi}}+\frac{T^n_{ozk+\frac{1}{2}}}{T^n_{o\varphi}}+\frac{T^n_{wzk+\frac{1}{2}}}{T^n_{w\varphi}}+\frac{T^n_{oyj+\frac{1}{2}}}{T^n_{o\varphi}}+ \frac{T^n_{wyj+\frac{1}{2}}}{T^n_{w\varphi}}+\frac{T^n_{oxi+\frac{1}{2}}}{T^n_{o\varphi}}+\frac{T^n_{wxi+\frac{1}{2}}}{T^n_{w\varphi}}+\frac{T^n_{o\beta}}{T^n_{o\varphi}}+\frac{T^n_{w\beta}}{T^n_{w\varphi}},$$

$e_{i,j,k+1}=\frac{T^n_{ozk+\frac{1}{2}}}{T^n_{o\phi}}+\frac{T^n_{wzk+\frac{1}{2}}}{T^n_{w\phi}}$, $f_{i,j+1,k}=\frac{T^n_{oyj+\frac{1}{2}}}{T^n_{o\phi}}+\frac{T^n_{wyj+\frac{1}{2}}}{T^n_{w\phi}}$, $g_{i+1,j,k}=\frac{T^n_{oxi+\frac{1}{2}}}{T^n_{o\phi}}+\frac{T^n_{wxi+\frac{1}{2}}}{T^n_{w\phi}}$,

$$H_{i,j,k}=\frac{T^{n}_{\mathrm{w}xi+\frac{1}{2}}}{T^{n}_{\mathrm{w}\phi}}p^{n}_{\mathrm{c},i+1,j,k}+\frac{T^{n}_{\mathrm{w}xi-\frac{1}{2}}}{T^{n}_{\mathrm{w}\phi}}p^{n}_{\mathrm{c},i-1,j,k}+\frac{T^{n}_{\mathrm{w}yj+\frac{1}{2}}}{T^{n}_{\mathrm{w}\phi}}p^{n}_{\mathrm{c},i,j+1,k}+\frac{T^{n}_{\mathrm{w}yj-\frac{1}{2}}}{T^{n}_{\mathrm{w}\phi}}p^{n}_{\mathrm{c},i,j-1,k}+$$
$$\frac{T^{n}_{\mathrm{w}zk+\frac{1}{2}}}{T^{n}_{\mathrm{w}\phi}}p^{n}_{\mathrm{c},i,j,k+1}+\frac{T^{n}_{\mathrm{w}zk-\frac{1}{2}}}{T^{n}_{\mathrm{w}\phi}}p^{n}_{\mathrm{c},i,j,k-1}-(\frac{T^{n}_{\mathrm{w}xi+\frac{1}{2}}}{T^{n}_{\mathrm{w}\phi}}+\frac{T^{n}_{\mathrm{w}xi-\frac{1}{2}}}{T^{n}_{\mathrm{w}\phi}}+\frac{T^{n}_{\mathrm{w}yj+\frac{1}{2}}}{T^{n}_{\mathrm{w}\phi}}+\frac{T^{n}_{\mathrm{w}yj-\frac{1}{2}}}{T^{n}_{\mathrm{w}\phi}}+\frac{T^{n}_{\mathrm{w}zk+\frac{1}{2}}}{T^{n}_{\mathrm{w}\phi}}+$$
$$\frac{T^{n}_{\mathrm{w}zk-\frac{1}{2}}}{T^{n}_{\mathrm{w}\phi}})p^{n}_{\mathrm{c},i,j,k}+\frac{TT^{n}_{\mathrm{o}zk+\frac{1}{2}}}{T^{n}_{\mathrm{o}\phi}}-\frac{TT^{n}_{\mathrm{o}zk-\frac{1}{2}}}{T^{n}_{\mathrm{o}\phi}}+\frac{TT^{n}_{\mathrm{w}zk+\frac{1}{2}}}{T^{n}_{\mathrm{w}\phi}}-\frac{TT^{n}_{\mathrm{w}zk-\frac{1}{2}}}{T^{n}_{\mathrm{w}\phi}}-(\frac{T^{n}_{\mathrm{o}\beta}}{T^{n}_{\mathrm{o}\phi}}+\frac{T^{n}_{\mathrm{w}\beta}}{T^{n}_{\mathrm{w}\phi}})p^{n}_{\mathrm{o},i,j,k}+\frac{T^{\mathrm{n}}_{\mathrm{oco1}}}{T^{n}_{\mathrm{o}\phi}}-$$
$$\frac{Q^{n}_{\mathrm{o},i,j,k}C^{n}_{\mathrm{o}1,i,j,k}}{T^{n}_{\mathrm{o}\phi}}+\frac{T^{\mathrm{n}}_{\mathrm{wcw1}}}{T^{n}_{\mathrm{w}\phi}}-\frac{Q^{n}_{\mathrm{w},i,j,k}C^{n}_{\mathrm{w}2,i,j,k}}{T^{n}_{\mathrm{w}\phi}}-\frac{T^{n}_{\mathrm{w}\beta}}{T^{n}_{\mathrm{w}\phi}}(p^{n+1}_{\mathrm{c},i,j,k}-p^{n}_{\mathrm{c},i,j,k})-$$
$$(\frac{T^{n}_{\mathrm{o},xi+\frac{1}{2}}}{T^{n}_{\mathrm{o}\phi}}+\frac{T^{n}_{\mathrm{w},xi+\frac{1}{2}}}{T^{n}_{\mathrm{w}\phi}})(\pm\Delta x_{i+\frac{1}{2}}\mathrm{D}^{n}_{\mathrm{P},i+\frac{1}{2},j,k})-(\frac{T^{n}_{\mathrm{o},xi-\frac{1}{2}}}{T^{n}_{\mathrm{o}\phi}}+\frac{T^{n}_{\mathrm{w},xi-\frac{1}{2}}}{T^{n}_{\mathrm{w}\phi}})(\pm\Delta x_{i-\frac{1}{2}}\mathrm{D}^{n}_{\mathrm{P},i-\frac{1}{2},j,k})-$$
$$(\frac{T^{n}_{\mathrm{o},yj+\frac{1}{2}}}{T^{n}_{\mathrm{o}\phi}}+\frac{T^{n}_{\mathrm{w},yj+\frac{1}{2}}}{T^{n}_{\mathrm{w}\phi}})(\pm\Delta y_{j+\frac{1}{2}}\mathrm{D}^{n}_{\mathrm{P},i,j+\frac{1}{2},k})-(\frac{T^{n}_{\mathrm{o},yj-\frac{1}{2}}}{T^{n}_{\mathrm{o}\phi}}+\frac{T^{n}_{\mathrm{w},yj-\frac{1}{2}}}{T^{n}_{\mathrm{w}\phi}})(\pm\Delta y_{j-\frac{1}{2}}\mathrm{D}^{n}_{\mathrm{P},i,j-\frac{1}{2},k})-$$
$$(\frac{T^{n}_{\mathrm{o},zk+\frac{1}{2}}}{T^{n}_{\mathrm{o}\phi}}+\frac{T^{n}_{\mathrm{w},zk+\frac{1}{2}}}{T^{n}_{\mathrm{w}\phi}})(\pm\Delta z_{k+\frac{1}{2}}\mathrm{D}^{n}_{\mathrm{P},i,j,k+\frac{1}{2}})-(\frac{T^{n}_{\mathrm{o},zk-\frac{1}{2}}}{T^{n}_{\mathrm{o}\phi}}+\frac{T^{n}_{\mathrm{w},zk-\frac{1}{2}}}{T^{n}_{\mathrm{w}\phi}})(\pm\Delta z_{k-\frac{1}{2}}\mathrm{D}^{n}_{\mathrm{P},i,j,k-\frac{1}{2}})$$

3.3. The difference equations for saturation

The saturation difference equations are:

$$s^{n+1}_{\mathrm{w},i,j,k}=\frac{(T^{n}_{\mathrm{w},xi+\frac{1}{2}}+T^{n}_{\mathrm{o},xi+\frac{1}{2}})(p^{n+1}_{\mathrm{o},i+1,j,k}-p^{n+1}_{\mathrm{o},i,j,k}\pm\Delta x_{i+\frac{1}{2}}\mathrm{D}^{n}_{\mathrm{P},i+\frac{1}{2},j,k})}{(T^{n}_{\mathrm{w}\phi}-T^{n}_{\mathrm{o}\phi})}+$$
$$\frac{(T^{n}_{\mathrm{w},xi-\frac{1}{2}}+T^{n}_{\mathrm{o},xi-\frac{1}{2}})(p^{n+1}_{\mathrm{o},i-1,j,k}-p^{n+1}_{\mathrm{o},i,j,k}\pm\Delta x_{i-\frac{1}{2}}\mathrm{D}^{n}_{\mathrm{P},i-\frac{1}{2},j,k})}{(T^{n}_{\mathrm{w}\phi}-T^{n}_{\mathrm{o}\phi})}+$$
$$\frac{(T^{n}_{\mathrm{w},yj+\frac{1}{2}}+T^{n}_{\mathrm{o},yj+\frac{1}{2}})(p^{n+1}_{\mathrm{o},i,j+1,k}-p^{n+1}_{\mathrm{o},i,j,k}\pm\Delta y_{j+\frac{1}{2}}\mathrm{D}^{n}_{\mathrm{P},i,j+\frac{1}{2},k})}{(T^{n}_{\mathrm{w}\phi}-T^{n}_{\mathrm{o}\phi})}+$$
$$\frac{(T^{n}_{\mathrm{w},yj-\frac{1}{2}}+T^{n}_{\mathrm{o},yj-\frac{1}{2}})(p^{n+1}_{\mathrm{o},i,j-1,k}-p^{n+1}_{\mathrm{o},i,j,k}\pm\Delta y_{j-\frac{1}{2}}\mathrm{D}^{n}_{\mathrm{P},i,j-\frac{1}{2},k})}{(T^{n}_{\mathrm{w}\phi}-T^{n}_{\mathrm{o}\phi})}+$$
$$\frac{(T^{n}_{\mathrm{w},zk+\frac{1}{2}}+T^{n}_{\mathrm{o},zk+\frac{1}{2}})(p^{n+1}_{\mathrm{o},i,j,k+1}-p^{n+1}_{\mathrm{o},i,j,k}\pm\Delta z_{k+\frac{1}{2}}\mathrm{D}^{n}_{\mathrm{P},i,j,k+\frac{1}{2}})}{(T^{n}_{\mathrm{w}\phi}-T^{n}_{\mathrm{o}\phi})}+$$

$$\frac{(T^{n}_{\mathrm{w},zk-\frac{1}{2}}+T^{n}_{\mathrm{o},zk-\frac{1}{2}})(p^{n+1}_{\mathrm{o},i,j,k-1}-p^{n+1}_{\mathrm{o},i,j,k}\pm\Delta z_{k-\frac{1}{2}}\mathrm{D}^{n}_{\mathrm{P},i,j,k-\frac{1}{2}})}{(T^{n}_{\mathrm{w}\phi}-T^{n}_{\mathrm{o}\phi})}-$$
$$\frac{T^{n}_{\mathrm{w},xi+\frac{1}{2}}(p^{n}_{\mathrm{c},i+1,j,k}-p^{n}_{\mathrm{c},i,j,k})}{(T^{n}_{\mathrm{w}\phi}-T^{n}_{\mathrm{o}\phi})}-\frac{T^{n}_{\mathrm{w},xi-\frac{1}{2}}(p^{n}_{\mathrm{c},i-1,j,k}-p^{n}_{\mathrm{c},i,j,k})}{(T^{n}_{\mathrm{w}\phi}-T^{n}_{\mathrm{o}\phi})}-\frac{T^{n}_{\mathrm{w},yj+\frac{1}{2}}(p^{n}_{\mathrm{c},i,j+1,k}-p^{n}_{\mathrm{c},i,j,k})}{(T^{n}_{\mathrm{w}\phi}-T^{n}_{\mathrm{o}\phi})}-$$
$$\frac{T^{n}_{\mathrm{w},yj-\frac{1}{2}}(p^{n}_{\mathrm{c},i,j-1,k}-p^{n}_{\mathrm{c},i,j,k})}{(T^{n}_{\mathrm{w}\phi}-T^{n}_{\mathrm{o}\phi})}-\frac{T^{n}_{\mathrm{w},zk+\frac{1}{2}}(p^{n}_{\mathrm{c},i,j,k+1}-p^{n}_{\mathrm{c},i,j,k})}{(T^{n}_{\mathrm{w}\phi}-T^{n}_{\mathrm{o}\phi})}-\frac{T^{n}_{\mathrm{w},zk-\frac{1}{2}}(p^{n}_{\mathrm{c},i,j,k-1}-p^{n}_{\mathrm{c},i,j,k})}{(T^{n}_{\mathrm{w}\phi}-T^{n}_{\mathrm{o}\phi})}-$$
$$\frac{(TT^{n}_{\mathrm{o},zk+\frac{1}{2}}+TT^{n}_{\mathrm{o},zk-\frac{1}{2}}-T^{n}_{\mathrm{w},zk+\frac{1}{2}}+T^{n}_{\mathrm{w},zk-\frac{1}{2}}-T^{n}_{\mathrm{oco1}}-T^{n}_{\mathrm{wcw2}})}{(T^{n}_{\mathrm{w}\phi}-T^{n}_{\mathrm{o}\phi})}-\frac{(T^{n}_{\mathrm{o}\beta}+T^{n}_{\mathrm{w}\beta})(P^{n+1}_{\mathrm{o},i,j,k}-P^{n}_{\mathrm{o},i,j,k})}{(T^{n}_{\mathrm{w}\phi}-T^{n}_{\mathrm{o}\phi})}+$$
$$\frac{(Q^{n}_{\mathrm{o},i,j,k}C^{n}_{\mathrm{o1},i,j,k}+Q^{n}_{\mathrm{w},i,j,k}C^{n}_{\mathrm{w2},i,j,k})}{(T^{n}_{\mathrm{w}\phi}-T^{n}_{\mathrm{o}\phi})}+s^{n}_{\mathrm{w},i,j,k} \tag{17}$$

3.4. The difference equations for concentrations

The difference equations for concentrations are:

$$A_{i+1,j,k}C_{\mathrm{w3},i+1,j,k}+B_{i-1,j,k}C_{\mathrm{w3},i-1,j,k}+C_{i,j+1,k}C_{\mathrm{w3},i,j+1,k}+D_{i,j-1,k}C_{\mathrm{w3},i,j-1,k}+$$
$$E_{i,j,k+1}C_{\mathrm{w3},i,j,k+1}+F_{i,j,k-1}C_{\mathrm{w3},i,j,k-1}+G_{i,j,k}C_{\mathrm{w3},i,j,k}=H \tag{18}$$

Where

$$A_{i+1,j,k}=\frac{1}{\Delta x_i}[\phi D_{\mathrm{o}3}s^{n+1}_{\mathrm{o},i+\frac{1}{2},j,k}\frac{2}{(\Delta x_i+\Delta x_{i+1})}\rho^{n+1}_{3,i+1,j,k}M+\phi D_{\mathrm{w}3}s^{n+1}_{\mathrm{w},i+\frac{1}{2},j,k}\frac{2}{(\Delta x_i+\Delta x_{i+1})}\rho^{n+1}_{3,i+1,j,k}+$$
$$M\lambda^{n}_{\mathrm{o},i+\frac{1}{2},j,k}\frac{2(p^{n+1}_{\mathrm{o},i+1,j,k}-p^{n+1}_{\mathrm{o},i,j,k}\pm\Delta x_{i+\frac{1}{2}}\mathrm{D}^{n}_{\mathrm{P}i+\frac{1}{2},j,k})}{(\Delta x_i+\Delta x_{i+1})}+\lambda^{n}_{\mathrm{w},i+\frac{1}{2},j,k}\frac{2(p^{n+1}_{\mathrm{w},i+1,j,k}-p^{n+1}_{\mathrm{w},i,j,k}\pm\Delta x_{i+\frac{1}{2}}\mathrm{D}^{n}_{\mathrm{P}i+\frac{1}{2},j,k})}{(\Delta x_i+\Delta x_{i+1})}],$$

$$B_{i-1,j,k}=\frac{1}{\Delta x_i}[\phi D_{\mathrm{o}3}s^{n+1}_{\mathrm{o},i-\frac{1}{2},j,k}\frac{2}{(\Delta x_i+\Delta x_{i-1})}\rho^{n+1}_{3,i-1,j,k}M+\phi D_{\mathrm{w}3}s^{n+1}_{\mathrm{w},i-\frac{1}{2},j,k}\frac{2}{(\Delta x_i+\Delta x_{i-1})}\rho^{n+1}_{3,i-1,j,k}-$$
$$M\lambda^{n}_{\mathrm{o},i-\frac{1}{2},j,k}\frac{2(p^{n+1}_{\mathrm{o},i-1,j,k}-p^{n+1}_{\mathrm{o},i,j,k}\pm\Delta x_{i-\frac{1}{2}}\mathrm{D}^{n}_{\mathrm{P}i-\frac{1}{2},j,k})}{(\Delta x_i+\Delta x_{i-1})}-\lambda^{n}_{\mathrm{w},i-\frac{1}{2},j,k}\frac{2(p^{n+1}_{\mathrm{w},i-1,j,k}-p^{n+1}_{\mathrm{w},i,j,k}\pm\Delta x_{i-\frac{1}{2}}\mathrm{D}^{n}_{\mathrm{P}i-\frac{1}{2},j,k})}{(\Delta x_i+\Delta x_{i-1})}],$$

$$C_{i,j+1,k}=\frac{1}{\Delta y_j}[\phi D_{\mathrm{o}3}s^{n+1}_{\mathrm{o},i,j+\frac{1}{2},k}\frac{2}{(\Delta y_j+\Delta y_{j+1})}\rho^{n+1}_{3,i,j+1,k}M+\phi D_{\mathrm{w}3}s^{n+1}_{\mathrm{w},i,j+\frac{1}{2},k}\frac{2}{(\Delta y_j+\Delta y_{j+1})}\rho^{n+1}_{3,i,j+1,k}+$$
$$M\lambda^{n}_{\mathrm{o},i,j+\frac{1}{2},k}\frac{2(p^{n+1}_{\mathrm{o},i,j+1,k}-p^{n+1}_{\mathrm{o},i,j,k}\pm\Delta y_{j+\frac{1}{2}}\mathrm{D}^{n}_{\mathrm{P}i,j+\frac{1}{2},k})}{(\Delta y_j+\Delta y_{j+1})}+\lambda^{n}_{\mathrm{w},i,j+\frac{1}{2},k}\frac{2(p^{n+1}_{\mathrm{w},i,j+1,k}-p^{n+1}_{\mathrm{w},i,j,k}\pm\Delta y_{j+\frac{1}{2}}\mathrm{D}^{n}_{\mathrm{P}i,j+\frac{1}{2},k})}{(\Delta y_j+\Delta y_{j+1})}],$$

$$D_{i,j-1,k}=\frac{1}{\Delta y_j}[\phi D_{o3}s^{n+1}_{3,i,j-\frac{1}{2},k}\frac{2}{(\Delta y_j+\Delta y_{j-1})}\rho^{n+1}_{o,i,j-1,k}M+\phi D_{w3}s^{n+1}_{w,i,j-\frac{1}{2},k}\frac{2}{(\Delta y_j+\Delta y_{j-1})}\rho^{n+1}_{3,i,j-1,k}-$$

$$M\lambda^{n}_{o,i,j-\frac{1}{2},k}\frac{2(p^{n+1}_{o,i,j-1,k}-p^{n+1}_{o,i,j,k}\pm\Delta y_{j-\frac{1}{2}}\mathrm{D}^{n}_{\mathrm{P}i,j-\frac{1}{2},k})}{(\Delta y_j+\Delta y_{j-1})}-\lambda^{n}_{w,i,j-\frac{1}{2},k}\frac{2(p^{n+1}_{w,i,j-1,k}-p^{n+1}_{w,i,j,k}\pm\Delta y_{j-\frac{1}{2}}\mathrm{D}^{n}_{\mathrm{P}i,j-\frac{1}{2},k})}{(\Delta y_j+\Delta y_{j-1})}],$$

$$E_{i,j,k+1}=\frac{1}{\Delta z_k}\{\varphi D_{o3}s^{n+1}_{o,i,j,k+\frac{1}{2}}\frac{2}{(\Delta z_k+\Delta z_{k+1})}\rho^{n+1}_{3,i,j,k+1}M+\varphi D_{w3}s^{n+1}_{w,i,j,k+\frac{1}{2}}\frac{2}{(\Delta z_k+\Delta z_{k+1})}\rho^{n+1}_{3,i,j,k+1}$$

$$+M\lambda^{n}_{o,i,j,k+\frac{1}{2}}[\frac{2(p^{n+1}_{o,i,j,k+1}-p^{n+1}_{o,i,j,k}\pm\Delta z_{k+\frac{1}{2}}\mathrm{D}^{n}_{\mathrm{P}i,j,k+\frac{1}{2}})}{(\Delta z_k+\Delta z_{k+1})}-\rho^{n+1}_{o,i,j,k+\frac{1}{2}}g]+$$

$$\lambda^{n}_{w,i,j,k+\frac{1}{2}}[\frac{2(p^{n+1}_{w,i,j,k+1}-p^{n+1}_{w,i,j,k}\pm\Delta z_{k+\frac{1}{2}}\mathrm{D}^{n}_{\mathrm{P}i,j,k+\frac{1}{2}})}{(\Delta z_k+\Delta z_{k+1})}-\rho^{n+1}_{w,i,j,k+\frac{1}{2}}g]\},$$

$$F_{i,j,k-1}=\frac{1}{\Delta z_k}\{\varphi D_{o3}s^{n+1}_{o,i,j,k-\frac{1}{2}}\frac{2}{(\Delta z_k+\Delta z_{k-1})}\rho^{n+1}_{3,i,j,k-1}M+\varphi D_{w3}s^{n+1}_{w,i,j,k-\frac{1}{2}}\frac{2}{(\Delta z_k+\Delta z_{k-1})}\rho^{n+1}_{3,i,j,k-1}$$

$$-M\lambda^{n}_{o,i,j,k-\frac{1}{2}}[\frac{2(p^{n+1}_{o,i,j,k-1}-p^{n+1}_{o,i,j,k}\pm\Delta z_{k-\frac{1}{2}}\mathrm{D}^{n}_{\mathrm{P}i,j,k-\frac{1}{2}})}{(\Delta z_k+\Delta z_{k-1})}-\rho^{n+1}_{o,i,j,k-\frac{1}{2}}g]-$$

$$\lambda^{n}_{w,i,j,k-\frac{1}{2}}[\frac{2(p^{n+1}_{w,i,j,k-1}-p^{n+1}_{w,i,j,k}\pm\Delta z_{k-\frac{1}{2}}\mathrm{D}^{n}_{\mathrm{P}i,j,k-\frac{1}{2}})}{(\Delta z_k+\Delta z_{k-1})}-\rho^{n+1}_{w,i,j,k-\frac{1}{2}}g]\},$$

$$G_{i,j,k}=-\frac{1}{\Delta x_i}\phi\{D_{o3}\rho^{n+1}_{3,i,j,k}M[\frac{2s^{n+1}_{o,i+\frac{1}{2},j,k}}{(\Delta x_i+\Delta x_{i+1})}+\frac{2s^{n+1}_{o,i-\frac{1}{2},j,k}}{(\Delta x_i+\Delta x_{i-1})}]+D_{w3}\rho^{n+1}_{3,i,j,k}[\frac{2s^{n+1}_{w,i+\frac{1}{2},j,k}}{(\Delta x_i+\Delta x_{i+1})}+\frac{2s^{n+1}_{w,i-\frac{1}{2},j,k}}{(\Delta x_i+\Delta x_{i-1})}]\}-$$

$$\frac{1}{\Delta y_j}\phi\{D_{o3}\rho^{n+1}_{3,i,j,k}M[\frac{2s^{n+1}_{o,i,j+\frac{1}{2},k}}{(\Delta y_j+\Delta y_{j+1})}+\frac{2s^{n+1}_{o,i,j-\frac{1}{2},k}}{(\Delta y_j+\Delta y_{j-1})}]+D_{w3}\rho^{n+1}_{3,i,j,k}[\frac{2s^{n+1}_{w,i,j+\frac{1}{2},k}}{(\Delta y_j+\Delta y_{j+1})}+\frac{2s^{n+1}_{w,i,j-\frac{1}{2},k}}{(\Delta y_j+\Delta y_{j-1})}]\}-$$

$$\frac{1}{\Delta z_k}\phi\{D_{o3}\rho^{n+1}_{3,i,j,k}M[\frac{2s^{n+1}_{o,i,j,k+\frac{1}{2}}}{(\Delta z_k+\Delta z_{k+1})}+\frac{2s^{n+1}_{o,i,j,k-\frac{1}{2}}}{(\Delta z_k+\Delta z_{k-1})}]+D_{w3}\rho^{n+1}_{3,i,j,k}[\frac{2s^{n+1}_{w,i,j,k+\frac{1}{2}}}{(\Delta z_k+\Delta z_{k+1})}+\frac{2s^{n+1}_{w,i,j,k-\frac{1}{2}}}{(\Delta z_k+\Delta z_{k-1})}]\}+$$

$$\{[-(C_p+C_o)M\phi\rho^{n+1}_{3,i,j,k}s^{n+1}_{w,i,j,k}+(C_p+C_w)\phi\rho^{n+1}_{3,i,j,k}s^{n+1}_{w,i,j,k}]\cdot\frac{P^{n+1}_{o.i.j.k}-P^{n}_{o.i.j.k}}{\Delta t^{n+1}}+(-M\phi\rho^{n+1}_{3,i,j,k}+\phi\rho^{n+1}_{3,i,j,k})\cdot$$

$$\frac{s^{n+1}_{w,i,j,k}-s^{n}_{w,i,j,k}}{\Delta t^{n+1}}\}-\frac{[M\phi\rho^{n+1}_{3,i,j,k}(1-s^{n+1}_{w,i,j,k})+\phi\rho^{n+1}_{3,i,j,k}s^{n+1}_{w,i,j,k}]}{\Delta t^{n+1}}$$

$$H=-\frac{[M\varphi\rho^{n+1}_{o,i,j,k}(1-s^{n+1}_{w,i,j,k})+\varphi\rho^{n+1}_{w,i,j,k}s^{n+1}_{w,i,j,k}]\cdot C^{n}_{w3.i.j.k}}{\Delta t^{n+1}}+a^{n}_{o3}\rho^{n+1}_{o,i,j,k}C_o+\rho^{n+1}_{o,i,j,k}\cdot a''^{n}_{o3}\cdot\frac{C^{n+1}_{o3,i,j,k}-C^{n}_{o3,i,j,k}}{\Delta t^{n+1}}$$

$$+a^{n}_{w3}\rho^{n+1}_{w,i,j,k}C_w+\rho^{n+1}_{w,i,j,k}\cdot a''^{n}_{w3}\cdot\frac{C^{n+1}_{w3,i,j,k}-C^{n}_{w3,i,j,k}}{\Delta t^{n+1}}-\rho_o q^{n}_{o,i,j,k}MC^{n}_{w3.i.j.k}-\rho_w q^{n}_{w,i,j,k}C^{n}_{w3.i.j.k}$$

4. Treatment of Wells

In the numerical simulation, the computations for flow inputs from the wells are an important issue that affects the accuracy of the simulation. The Peaceman's well model is adopted in this paper to describe the relations for borehole bottom pressure, the pressures of the grid blocks that involve wells, and the production rate.

For production well:

$$p_{\mathrm{wf}} = p_{\mathrm{o}} - \frac{q\mu}{2\pi(k_{\mathrm{x}}k_{\mathrm{y}})^{\frac{1}{2}}\Delta z}\ln\frac{r_{\mathrm{o}}}{r_{\mathrm{w}}} - r_{\mathrm{o}}\mathrm{D}_{\mathrm{p}} \tag{19}$$

For water injection well:

$$p_{\mathrm{wf}} = p_{\mathrm{o}} - \frac{q\mu}{2\pi(k_{\mathrm{x}}k_{\mathrm{y}})^{\frac{1}{2}}\Delta z}\ln\frac{r_{\mathrm{o}}}{r_{\mathrm{w}}} + r_{\mathrm{o}}\mathrm{D}_{\mathrm{p}} \tag{20}$$

With r_{o} the equivalent radius for the well block, generally, for uniform rectangular grid block and taking into account the anisotropy, we have:

$$r_{\mathrm{o}} = \frac{0.14[(k_{\mathrm{y}}/k_{\mathrm{x}})^{\frac{1}{2}}\Delta x^2 + (k_{\mathrm{x}}/k_{\mathrm{y}})^{\frac{1}{2}}\Delta y^2]^{\frac{1}{2}}}{0.5[(k_{\mathrm{y}}/k_{\mathrm{x}})^{\frac{1}{4}} + (k_{\mathrm{x}}/k_{\mathrm{y}})^{\frac{1}{4}}]} \tag{21}$$

The production index is:

$$PID = \frac{2\pi k\Delta z}{\ln[r_{\mathrm{o}}/r_{\mathrm{w}}] + s} \tag{22}$$

In the numerical simulation, two cases are considered for the production rate: fixed production rate and fixed production pressure.

4.1. Production with fixed production rate

A. Fixed liquid production rate

For a given overall liquid production rate Q_{VT} for some well with N production layers, the overall mobility and phase mobility of each layer are:

$$\lambda_{\mathrm{T}k} = \left(\frac{k_{\mathrm{ro}}}{\mu_{\mathrm{o}}B_{\mathrm{o}}} + \frac{k_{\mathrm{rw}}}{\mu_{\mathrm{w}}B_{\mathrm{w}}}\right)_k \tag{23}$$

$$\lambda_{\mathrm{l}k} = \left(\frac{k_{\mathrm{rl}}}{\mu_{\mathrm{l}}B_{\mathrm{l}}}\right)_k \tag{24}$$

Therefore, the underground production rate for the some phase in the k^{th} layer is:

$$Q_{\mathrm{l}} = Q_{\mathrm{VT}} \cdot (PID_k \cdot \lambda_{\mathrm{l}k}) \cdot B_{\mathrm{l}} / \sum_{k=1}^{N}(PID_k \cdot \lambda_{\mathrm{T}k}) \tag{25}$$

B. Fixed oil production rate

Given ground oil production rate Q_{o} for a single well with N production layers, the underground production rate for the k^{th} layer is:

$$Q_{\mathrm{o}}(k) = Q_{\mathrm{o}} \cdot PID_k \cdot \lambda_{\mathrm{o}k} \cdot B_{\mathrm{o}} \Big/ \sum_{k=1}^{N}(PID_k \cdot \lambda_{\mathrm{o}k}) \tag{26}$$

$$Q_{\mathrm{w}}(k) = Q_{\mathrm{o}}(k)(\frac{k_{\mathrm{rw}}}{\mu_{\mathrm{w}}})_k \Big/ (\frac{k_{\mathrm{ro}}}{\mu_{\mathrm{o}}})_k \tag{27}$$

C. Water injection well. Given injection rate Q_{w}, the injection rate at the k^{th} layer is:

$$Q_{\mathrm{w}}(k) = Q_{\mathrm{w}} \cdot PID_k \, \lambda_{\mathrm{T}k} \cdot B_{\mathrm{w}} \Big/ \sum_{k=1}^{N} (PID_k \cdot \lambda_{\mathrm{T}k}) \tag{28}$$

4.2. Production with fixed bottom hole pressure

A. Production wells

$$Q_{\mathrm{o}}(K) = PID_k (\frac{K_{\mathrm{ro}}}{\mu_{\mathrm{o}}})_k (p_k - p_{\mathrm{wf}k} - r_{\mathrm{o}} \mathrm{D}_{\mathrm{p}}) \tag{29}$$

$$Q_{\mathrm{w}}(k) = Q_{\mathrm{o}}(k)(\frac{K_{\mathrm{rw}}}{\mu_{\mathrm{w}}})_k \Big/ (\frac{k_{\mathrm{ro}}}{\mu_{\mathrm{o}}})_k \tag{30}$$

B. Water injection wells

$$Q_{\mathrm{w}}(k) = PID_k \cdot \lambda_{\mathrm{T}k} (p_k - p_{\mathrm{wf}k} + r_{\mathrm{o}} \mathrm{D}_{\mathrm{p}}) \tag{31}$$

5. Treatment of the Adsorption of the Surfactant

The adsorption of the surfactant to the solid/liquid interface is one of the major reasons for the loss of surfactant, which directly influences the oil displacement efficiency of the surfactant [12]. The core adsorption experiments for surfactants show that the adsorption of surfactants satisfies the Langmuir isotheral adsorption equation. The equation considers the effects from salinity, concentrations of surfactants, and permeability of rocks. The adsorption process is irreversible to the concentrations of surfactants, but reversible for salinity. The equation can be written as:

$$C_{\mathrm{r}} = bC_{\mathrm{rm}}C / (1 + bC) \tag{32}$$

A large number of experiments prove that the amount of adsorbed surfactants linearly increases with the increase of the effective salinity and linearly decreases with the increase of permeability. The empirical relation is:

$$a = bC_{\mathrm{rm}} = (aa_1 + aa_2 \cdot C_{\mathrm{se}}) \cdot k^{0.5} \tag{33}$$

The adsorption parameters b, aa_1 and aa_2 are obtained by regressions from the experiment data.

In the current available chemical flooding numerical simulation software, the adsorption concentration (the percentage of the volume of the surfactant that is adsorbed on the surface of the rock pores in the volume of the pores) is generally used to express the magnitude of the amount of adsorption. The calculation is based on the Langmuir isothermal adsorption equation where the concentration C in the equation is the average concentration of the surfactant in each phase. This computation approach results in large discrepancies. The reason is that during the surfactant flooding, the saturations in oil and water phase change with time and therefore, the concentrations of the surfactant in both phases change with time as well. Experimental data show that the adsorption rate for the surfactant is different in oil phase and water phase. The determinant of the adsorption parameters is usually conducted in pores which are saturated by single phase (oil or water) fluid. Therefore, in this paper, when calculating the adsorbance for the surfactant, the calculation for the adsorbance from the oil phase is separated from that from the water phase. The fact that there is only part of the solid particles contact with the i^{th} phase is reflected by a function $B_{\mathrm{i}}(s_{\mathrm{i}})$ in the calculation of the adsorbance of surfactant in oil and water phase, which is:

$$a_{o3} = B_o(s_o)C_{or}(C_{o3}) \tag{34}$$

$$a_{w3} = B_w(s_w)C_{wr}(C_{w3}) \tag{35}$$

$$C_{or}(C_{o3}) = b_o C_{om} C_{o3} / (1 + b_o C_{o3}) \tag{36}$$

$$C_{wr}(C_{w3}) = b_w C_{wm} C_{w3} / (1 + b_w C_{w3}) \tag{37}$$

Where the dimensionless function $B_i(s_i)$ is determined from experiments and satisfies the following conditions: $B_i(0) = 0$, $B_i(1) = 1$.

6. Treatment for Relative Permeability Curves

The major mechanism for the increase of recovery by surfactant solution flooding is that the surface tension at the oil water interface is decreased so that the oil drops are more likely to deform to flow through pore throats and the adhesion of the crude oil to the surface of rocks reduces as well [13-15]. On the macro level, surfactant flooding raises the relative permeability curve of the oil phase. Therefore, in the numerical simulation of surfactant flooding, properly expressing the relation between the oil-water relative permeability and the concentration of the surfactant is crucial to the accuracy of the numerical simulation results. In the programming of the software with the proposed method, two choices are given for the calculation of the relative permeability at different surfactant concentration. The first one based on the interpolations from experimental relative permeability curves for several different concentrations. The other one performs the calculation based on the theoretical formula. Since the interpolation method bases itself on experimental results, it is advantageous in good matching to the real data, which should be selected first. However, the method needs a great amount of experimental data. When few relative permeability curves are available, calculations have to be performed using the theoretical formula.

6.1. Interpolation

N experimental relative permeability curves for different concentrations are input to the data stream. Assuming that the surfactant concentration that corresponds to the i^{th} relative permeability curve is C_{w3i}, normalizations can be done on the saturations of the curves:

$$s_{oNi} = \frac{s_o - s_{ori}}{1 - s_{wc} - s_{ori}} \tag{38}$$

$$s_{wNi} = \frac{s_w - s_{wc}}{1 - s_{wc} - s_{ori}} \tag{39}$$

If the surfactant concentration for some point in the reservoir is C_{w3x}, which is between C_{w3i} (the i^{th} relative permeability curve) and C_{w3i+1} (i+1th relative permeability curve), then the corresponding relative permeability should be calculated by interpolation. The procedure goes as follows. First, the residual oil saturation s_{orx} at the concentration is calculated.

$$s_{orx} = s_{ori} + \frac{C_{w3x} - C_{w3i}}{C_{w3i+1} - C_{w3i}}(s_{ori+1} - s_{ori}) \tag{40}$$

$$s_{oNx} = \frac{s_o - s_{orx}}{1 - s_{wc} - s_{orx}} \tag{41}$$

$$s_{wNx} = \frac{s_w - s_{wc}}{1 - s_{wc} - s_{orx}} \tag{42}$$

At s_{oNx}, the oil phase relative permeability on the i^{th} and the $(i+1)^{th}$ curves are K_{roxi} and K_{roxi+1}. The oil phase relative permeability when the concentration is C_{w3x} and the saturation is s_o, then:

$$K_{rox} = K_{roxi} + \frac{C_{w3x} - C_{w3i}}{C_{w3i+1} - C_{w3i}}(K_{roxi+1} - K_{roxi}) \tag{43}$$

The interpolation for the water phase relative permeability is identical to that for the oil phase.

6.2. Theoretical Formula

The theoretical method uses less experimental data and can be universally applied, but the error between the calculated value and the real one can be large. The formula is:

$$K_{lr} = K_{lr}^{o} \cdot (s_{lN})^{n_l} \tag{44}$$

Where the subscript *l* can be either o or w and s_{lN} is the normalized saturation. The endpoint value K_{lr}^{o} and the exponent n_l are determined by interpolation from input data.

$$K_{lr}^{0} = K_{lr}^{0,low} + \frac{s_{or} - s_{or}^{low}}{s_{or}^{high} - s_{or}^{low}}(K_{lr}^{0,high} - K_{lr}^{0,low}) \tag{45}$$

$$n_l = n_l^{low} + \frac{s_{or} - s_{or}^{low}}{s_{or}^{high} - s_{or}^{low}}(n_l^{high} - k_l^{low}) \tag{46}$$

Where: $s_{or} = s_{or}^{high} + \frac{s_{or}^{low} - s_{or}^{high}}{1 + T_o \cdot N_{To}}$, $N_{To} = \sqrt{N_{co}^2 + 2N_{co} \cdot N_{Bo} + N_{Bo}^2}$, $N_{co} = \frac{k \cdot \nabla p_w}{\sigma_{ow}}$

$N_{Bo} = \frac{kg(\rho_o - \rho_w)}{\sigma_{ow}}$.

The oil water interface surface tension σ_{ow} is determined by the surfactant concentration. Hence, the theoretical relation between the relative permeability and the surfactant concentration is established.

7. Development of the Surfactant Flooding Numerical Simulation Software

Based on the mathematical model of the surfactant flooding and treatments for different parameters, a three-dimension two-phase three-component surfactant flooding numerical simulation software is developed. The software is programmed by FOR90 language. It can simulate the development dynamic indices for water flooding and surfactant flooding in oil reservoirs when there are variations in the thickness of oil reservoirs in 3D space. The software also allows dead nodes where the effective thickness, the porosity, or the permeability is zero.

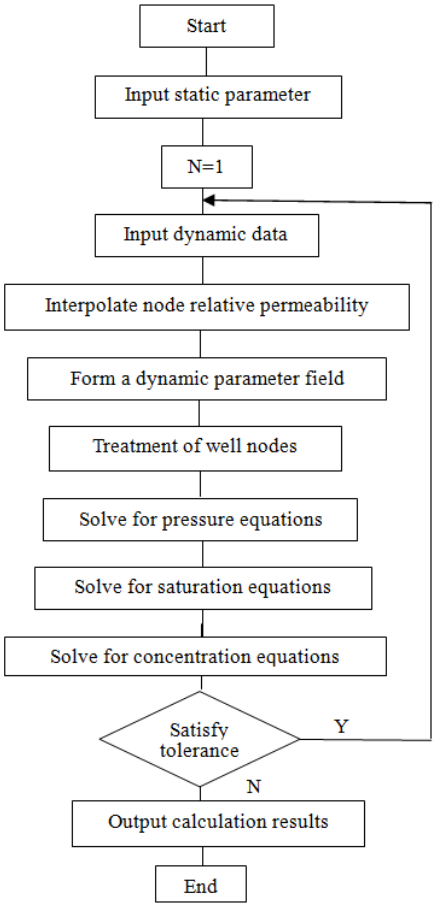

Figure 1. Flow chart of the solution algorithm

8. Oilfield Experiments for Surfactant Flooding

According to the laboratory data from the surfactant core flooding experiments, the oilfield experiment for surfactant injection was carried out on the Chao 61 district low permeability reservoirs. The alkanolamide nonionic surfactant mixture system that matches with the oil reservoir conditions was injected. With the help of the changes of the surface tension, the wettability, the viscosity, and the rheology, the goal to reduce the threshold pressure and establish effective driving pressure difference between oil and water wells is achieved. The production rate of low permeability reservoirs is improved.

8.1. An overview of the test area

1) The conditions for selected wells and reservoirs in the test area

(1) Formation conditions and development situations are relatively good;

(2) Water wells with high injection pressure and poor injection rate;

(3) Oil production rate about 1.0 t/d for neighborhood connecting oil wells;

(4) At least has one stably developing sand body;

(5) The injection water should be clear water during the test.

2) The results of well selection

According to the above conditions, the Chao 80-152 well area in the Chao 61 district was selected. In order to sufficiently explore the potential of production rate of residual oil in thin reservoirs, as of July 2011, for the four water wells in the test area, the average allocated injective pressure for a single well was 12.93MPa, the allocated injection amount was 26.25m^3, the real injection pressure was 12.93 MPa, the real injection amount was 19.53m^3, and the cumulative injection amount was 5.1081×10^4 m^3. The oil production wells were put into operation from January 2012 to June 2012. The average number of operation reservoirs for a single well was 29. The overall thickness was 20.1m. The effective thickness was 3.85m. The average daily liquid production was 15.0t for a single well. The daily oil production was 3.5t. The water cut was 76.7%. The submergence depth was 357m. The cumulative liquid production amount was 2.7933×10^4t. The cumulative oil production was 0.8242×10^4t. The average daily liquid production for single well was 13.8t for the related eight oil production wells (exclude Chao 84-152 due to shutdown). The daily oil production was 3.0t. The water cut was 78.2%. The submergence depth was 383m. The cumulative liquid production was 15.6905×10^4t and the cumulative oil production was 5.5873×10^4t.

Currently, the four water injection wells inject water near the burst pressure, where Chao 82-150 and Chao 82-152 cannot complete the assigned amount. Although Chao 82-154 operates under a hierarchical column, it cannot be used in the test due to low water injection rate. Chao 82-156 can only have an injection rate of 20m^3 due to top burst pressure, so it is not included in the test. The well data in the test area are shown in Table 1 and Table 2.

Table 1. Oil wells production data in the test area

Well	Initial stage			2011.7		
	Liquid production (t/d)	Oil production (t/d)	Water cut (%)	Liquid production (t/d)	Oil production (t/d)	Water cut (%)
C80-148	16	9	43.8	10	2	80
C80-150	27	11	59.3	29	7	75.9
C80-152	7	1	85.7	16	3	81.2
C80-154	8	5	37.5	5	2	60
C80-156	12	4	66.7	29	3	89.7
C84-148	14	10	28.6	11	6	45.5
C84-150	12	2	83.3	9	1	88.9
C84-152	3	0	100	0	0	0
C84-154	4	2	50	1	0	100
Average	11.4	4.9	57	13.8	3	78.2

Table 2. Conditions for water injection wells in the surfactant test area

Well	Sandstone thickness (m)	Fracture pressure (MPa)	Water injection pressure (MPa)	Assigned injection amount (m^3)	Daily injection (m^3)	Cumulative injection (m^3)
C82-150	21.5	12.6	12.6	30	22	17077
C82-152	12.6	13.3	13.3	30	10	7264
C82-154	24.3	12.5	12.5	25	22	14676
C82-156	19.7	13.3	13.3	20	20	9213
Average value	19.5	12.9	12.9	26.3	18.5	12058

8.2. Experiment plans

According to the water flooding numerical simulation results for Chao 82-152, the influences of the surfactant solution on the development performance for low permeability reservoir are studied with different surfactant concentration, slug length, and slug combination.

1) The determination of the concentration of surfactant

In order to analyze the effects of surfactant with different concentrations on the development performance of low permeability reservoir, the development index and water flooding recovery are first calculated under water flooding production conditions. Then four plans were designed for different concentrations of surfactants.

Plan 1: The slug concentration for the injected surfactant solution is 0.5%. The injected slug size is 0.02PV. Water flooding is continued after the injection of surfactant solution.

Plan 2: The slug concentration for the injected surfactant solution is 1.0%. The injected slug size is 0.02PV. Water flooding is continued after the injection of surfactant solution.

Plan 3: The slug concentration for the injected surfactant solution is 1.5%. The injected slug size is 0.02PV. Water flooding is continued after the injection of surfactant solution.

Plan 4: The slug concentration for the injected surfactant solution is 2.0%. The injected slug size is 0.02PV. Water flooding is continued after the injection of surfactant solution.

The surfactant flooding numerical simulation software is applied to calculate the development index for each plan. The indices are compared with those for water flooding. The calculation results are shown in Table 3. According to the simulation results, with the increase of the injected slug concentration, the final recovery gradually increases, but the amount of increases becomes smaller. The rational slug concentration should be determined combined with economical evaluations. The results after the economical evaluations show that the rational slug concentration is 0.5% from plan 1.

Table 3. The net income of plans with different slug concentrations

Plan	Concentration (%)	Injection amount (PV)	EOR (%)	△EOR (%)	Increasing in cost (10,000RMB)	Increasing in net income (10,000RMB)
Water flooding	/	/	32.34	/	/	/
Plan 1	0.5	0.01	33.22	0.88	18.5	217.6
Plan 2	1.0	0.01	33.41	1.07	35.0	211.0
Plan 3	1.5	0.01	33.53	1.19	51.5	202.2
Plan 4	2.0	0.01	33.59	1.25	68.0	192.5

2) The determination of the slug size of the surfactant

In order to investigate the influence of the slug size on the water flooding development performance for low permeability reservoir, the following four plans are designed.

Plan 5: The slug concentration for the injected surfactant solution is 0.5%. The injected slug size is 0.01PV. Water flooding is continued after the injection of surfactant solution.

Plan 6: The slug concentration for the injected surfactant solution is 0.5%. The injected slug size is 0.02PV. Water flooding is continued after the injection of surfactant solution.

Plan 7: The slug concentration for the injected surfactant solution is 0.5%. The injected slug size is 0.03PV. Water flooding is continued after the injection of surfactant solution.

Plan 8: The slug concentration for the injected surfactant solution is 0.5%. The injected slug size is 0.04PV. Water flooding is continued after the injection of surfactant solution.

The simulation results for the final recovery for plan 5 to 8 are shown in Table 4. According to the table, with the increase of slug length, the development performance becomes better and the recovery gradually increases. Since the surfactant flooding method used to produce the residual oil in low permeability reservoir is only at the testing stage, the development performance needs to be further examined. Therefore, the slug length should not be too large. With the consideration of economic constraints, the injected slug length is set to be 0.02PV in the teat area.

Table 4. The effects of different slug size on the recovery

	Water flooding	Plan 5	Plan 6	Plan 7	Plan 8
EOR(%)	32.34	32.86	33.22	33.50	33.68
ΔEOR(%)	/	0.52	0.88	1.16	1.34

3) The determination of surfactant slug combination

In order to study the influences of the surfactant slug combination on the development performance of low permeability reservoir, three plans are designed.

Plan 9: The slug concentration for the injected surfactant solution is 0.5%. The injected slug size is 0.02PV. Water flooding is continued after the injection of surfactant solution.

Plan 10: First, surfactant with 0.5% slug concentration and 0.01PV slug size is injected. Then normal water is injected with 0.01PV. After the water flooding, surfactant with 0.5% slug concentration and 0.01PV slug size is injected. Water flooding is carried out then.

Plan 11: First, surfactant with 0.5% slug concentration and 0.006PV slug size is injected. Then normal water is injected with 0.006PV. After the water flooding, surfactant with 0.5% slug concentration and 0.007PV slug size is injected. Then water flooding is carried out with 0.007PV. After the water flooding, surfactant with 0.5% slug concentration and 0.007PV slug size is injected. Water flooding is carried out then.

The final recovery and economic performances for Plan 9 to 15 are shown in Table 5. According to the simulation results, the multi-slug injection method yields better development performance than single slug, but the increase in recovery is limited. The recovery for three slugs is only 0.05% higher than a single slug. Taking into account that the multi-slug injection method increases the working load, it is not suggested to have many stages of slug injection.

Table 5. The net income for plans with different slug combinations

Plan	Concentration (%)	Injection amount (PV)	EOR (%)	ΔEOR (%)	Increasing in cost (10,000RMB)	Increasing in net income (10,000RMB)
Water flooding	/	/	32.34	/	/	/
Plan 9	0.5	0.02	33.22	0.88	18.5	217.6
Plan 10	0.5	0.02	33.25	0.91	20.5	216.2
Plan 11	0.5	0.02	33.27	0.93	22.5	214.5

Based on the numerical simulation results and the economic evaluations, the injection plan for the test area is determined. The surfactant concentration is 0.5%. The slug size is 0.02PV with a combination of two slugs, which alternated with water flooding.

Using the optimal plan for the surfactant slug parameters, the surfactant flooding numerical simulation is carried out for Chao 82-152 well area. The simulated concentration fields at different time for the fourth simulation layer are shown in Figure 2 and 3. The oil saturation fields for surfactant flooding and water flooding at different time are shown in Figure 4 to 7.

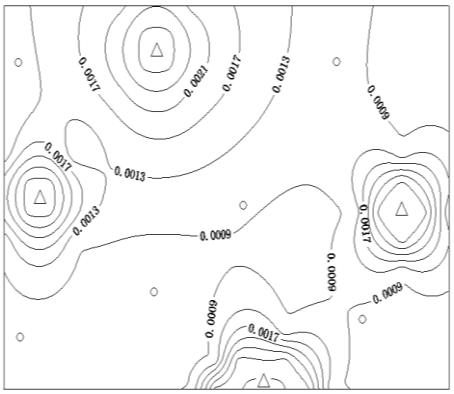

Figure 2. The surfactant distribution after 6 months of surfactant flooding

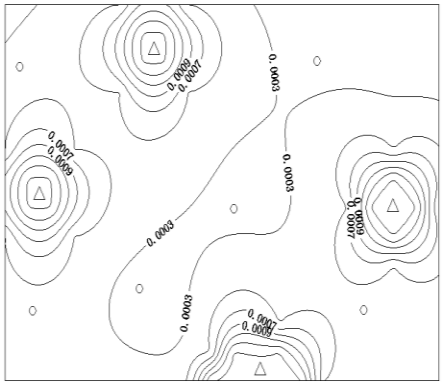

Figure 3. The surfactant distribution after 12 months of surfactant flooding

It can be seen from Figure 2 and 3 that after six months of the surfactant flooding, there is a significant decline in the concentration of the surfactant. The surfactant concentration reaches 0.3% around the injection wells, while the concentration reaches about 0.1% around the production rate. After 12 months, the surfactant concentration gradually decreases to an average value of 0.05%. It indicates that there no improvement on the production after a year of the surfactant flooding.

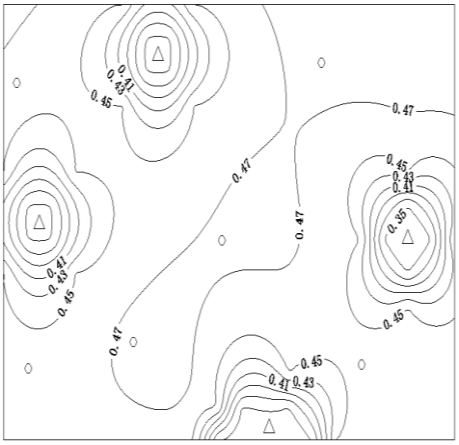

Figure 4. The oil saturation distribution after 6 months of water flooding

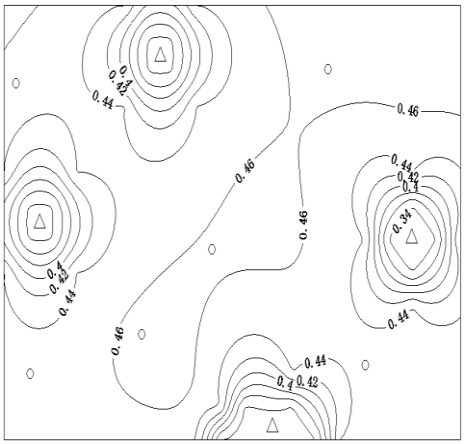

Figure 5. The oil saturation distribution after 12 months of water flooding

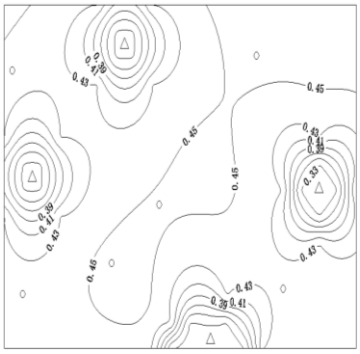

Figure 6. The oil saturation distribution after 6 months of surfactant flooding

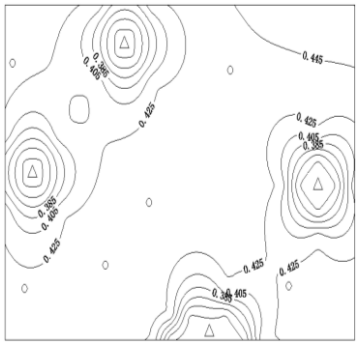

Figure 7. The oil saturation distribution after 12 months of surfactant flooding

It can be seen from Figure 4 to 7, after six months of surfactant flooding, the oil saturation is 0.02 lower than that for water flooding, which shows that the surfactant flooding increases the recovery.

8.3. Oilfield experimental results

8.3.1. The oilfield injection amount: The surfactant flooding injection experiment started from September 10th, 2011 and ended at December 5th. The experiment was conducted using the above optimal plan. The injection amount of pure surfactant to each well is shown in Table 6. The total amount of injection is 34t.

Table 6. The injection amount of pure surfactant to each injection well

Well	C82-150	C82-152	C82-154	C82-156
Injection amount(t)	5	8	14	7

8.3.2. Results and discussions of the oilfield experiment:

1) The threshold pressure decreases and the water absorption rate increases

Before the experiment, all of the flow pressures of the four water injection wells reached the burst pressure 23.5MPa. The overall daily water injection was 70m^3. The average daily water injection for single well was 17.5 m^3. In December, the average flow pressure of water injection wells reduced to 22.5MPa, but the daily water injection increased to 97 m^3. The average daily water injection for single well was 24.25 m^3. The comparisons of the surfactant experiment are shown in Table 7.

Table 7. Comparisons of performances of surfactant flooding experiment

Well	Before the experiment		The beginning of the experiment		After experiment (12 months)		Cumulative increase injected water (m^3)
	Pressure (MPa)	Water injection (m^3/d)	Pressure (MPa)	Water injection (m^3/d))	Pressure (MPa)	Water injection (m^3/d))	
C82-150	23.6	22	23.4	35	22.6	32	1675
C82-152	23.5	8	23.2	13	22.5	11	1628
C82-154	23.5	22	23.2	34	22.4	32	1490
C82-156	23.4	18	23.3	27	22.7	22	126
Total	23.5	70	23.3	109	22.5	97	4919

It can be seen from the water injection for a single well that the injection ability for all four wells increases. The daily water injection of Chao 82-150 increased from $22m^3$ to $35m^3$ and the increment lasts till now. The cumulative increment of the water injection is $1675m^3$. The water injection rate of Chao 82-152 only increased by $5m^3$ with a cumulative increment of water injection of $1628m^3$, but the effect has been vanished. The daily water injection rate for Chao 82-154 increased from $22m^3$ to $34m^3$. The cumulative increment of the water injection is $1490m^3$. Currently, the daily water injection rate is $23m^3$. The daily water injection rate increased from $18m^3$ to $27m^3$, but the increment only lasted for two months. The cumulative increment of water injection is $126m^3$. The total increment of the water injection is $4919m^3$ for all four wells.

2) The low permeability reservoir production ratio increased

The changes of low permeability reservoir production ratio are shown in Table 8. It can be seen from the table that the number of low permeability reservoir production layers increases to 14 from 9, which is the number before the experiment. The production ratio increases from 18.8% to 29.2%. The increment is 10.4%.

Table 8. Changes in the production for low permeability reservoir

Well	Perforated low permeability reservoirs (number)	Low permeability reservoir before the experiment		Low permeability reservoir after the experiment		Increase value	
		Production reservoirs (number)	Production ratio (%)	Production reservoirs (number)	Production ratio (%)	Production reservoirs (number)	Production ratio (%)
C82-150	25	1	4	5	20	4	16
C82-156	23	8	34.7	9	39.1	1	4.4
Total	48	9	18.8	14	29.2	5	10.4

3) The nearby oil wells started to be affected

The effects on the related oil production wells are shown in Table 9. There are five nearby related oil production wells being affected. The daily liquid production increased from 50t to 75t by 25t. The daily oil production increased from 14t to 18t by 4t. The water cut increased from 72% to 76%. The submergence depth reduced from 252m to 221m. The improvement in oil production lasts till now for the two oil wells, Chao 84-150 and Chao 84-154. The cumulative increment of oil production is 666t. The other three wells increase the liquid production capacity, which alleviates the decline of the production.

Table 9. Oil production effects for related oil wells

Well	Production capacity before the test				Production capacity after the effect				Cumulative increased amount of oil (t)
	Liquid (t)	Oil (t)	Water cut (%)	Submergence depth (m)	Liquid (t)	Oil (t)	Water cut (%)	Submergence depth (m)	
C80-152	12	2	83.3	76	18	2	86.9	61	0
C80-148	11	3	72.7	20	16	2	87.1	12	0
C84-150	15	2	86.7	273	25	4	83.3	142	248
C84-154	1	0	100	833	4	3	29.9	882	418
C84-148	11	7	36.4	56	12	7	41.7	9	0
Total	50	14	72.0	252	75	18	76.0	221	666

4) Evaluations on economic benefits

As of the end of June, 2012, the cumulative increase of the oil production for the two oil wells reached 971t. All five oil wells prevent the production rate from continuously declining by 1215t, which give a total of 2186t. The net economic profit is 1.32 million RMB. The investment and income ratio is 1:3.37.

9. Conclusions

1) A three-dimension two-phase three-component mathematical model was established for surfactant flooding. The difference equation was solved using implicit pressure and concentration terms and explicit saturation terms.

2) A new approach was used for the relation between the adsorbance of the surfactant and the relative permeability curve, which gave data that were closer to actual situations. The numerical simulation software for surfactant flooding was developed.

3) A numerical simulation study was carried out for Chao 61 district in Daqing Chaoyanggou oilfield. The surfactant injection plan was optimized and oilfield experiment was performed. The oilfield experiment results showed that after the injection of surfactant, the threshold pressure decreased and the water absorption capacity increased. The low permeability reservoirs production ratio increased and the related oil production wells started to be effected. The implementation of surfactant flooding had a decent performance both in oilfield development and economic benefits.

Acknowledgements

This work is supported by the National Natural Science Foundation of China under Grant No.51074034.

References

[1] D. Y. Yin, H. Pu and Y. X. Wu, "Numerical simulation of imbibition oil recovery for low permeability fractured reservoir", Chinese Journal of Hydrodynamics, vol. 4, **(2004)**, pp. 19.
[2] D. Y. Yin and H. Pu, "Numerical Simulation Study on Surfactant Flooding for Low Permeability Oilfield in The Condition of Threshold Pressure", Journal of Hydrodynamics, vol. 4, **(2008)**, pp. 20.
[3] D. Y. Yin, Y. G. Guo and W. M. Huang, "The determination of reasonable cycle time for bailing oil production in low permeability field" The 21st session of the national seminar on hydrodynamics and the 8th national conference on hydrodynamics and on both sides of the ship and ocean engineering hydrodynamics seminar, **(2008)** August, pp. 562-567; China.
[4] D. O. Son, H. J. Choi, H. G. Jeon and C. H. Kim, "Thermal-aware 3D Multi-core Process-or Design using Core and Level-2 Cache Placement", International Journal of Control and Automation, vol. 6, **(2013)**, pp. 25.
[5] A. Fouad, D. Boukhetela and F. Boudjema, "Decentralized Sliding Mode Controller Based on Genetic algorithm and a Hybrid approach for Interconnected Uncertain Nonlinear Systems", International Journal of Control and Automation, vol. 6, **(2013)**, pp. 61.
[6] J. Wang and M. Dong, "Simulation of O/W Emulsion Flow in Alkaline/Surfactant Flood for Heavy Oil Recovery", **(2010)** June; Journal of Canadian Petroleum Technology.
[7] Z. Xu, Y. Yin and J. Wang, "An Energy-efficient Clustering Algorithm in Wireless Sensor Networks with Multiple Sinks", International Journal of Control and Automation, vol. 5, (2012), pp. 131.
[8] Y. Kyung, J. -w. Kim, S. -B. Jung and K. -H. Eom, "Optimal Control Method for a Hydroelec-tric Power Development in Multi Level Dams", International Journal of Control and Automation, vol. 3, **(2009)**, pp. 13.
[9] S. M. Tripathi, T. S. Bholanath and S. Shantkriti, "Synthesis and Study of Applications of Metal coated Carbon Nanotubes", International Journal of Control and Automation, vol. 3, **(2010)**, pp. 53.
[10] R. D. Kokate and L. M. Waghmare, "Review of Tuning Methods of DMC and Performance Evaluation with PID Algorithms on a FOPDT Model", International Journal of Control and Automation, vol. 4, **(2011)**, pp. 95.

[11] A. Ansari, M. Haroun, N. A. Sayed, N. Al Kindy, B. Ali, R. A. Shrestha and H. Sarma, "A New Approach Optimizing Mature Waterfloods with Electrokinetics- Assisted Surfactant Flooding in Abu Dhabi Carbonate Reservoirs", **(2012)** December 10 - 12; 2012 SPE Kuwait International Petroleum Conference and Exhibition.
[12] H. H. Pei, G. C. Zhang, J. J. Ge, L. Ding, M. G. Tang and Y. F. Zheng, "A Comparative Study of Alkaline Flooding and Alkaline/Surfactant Flooding for Zhuangxi Heavy Oil", **(2012)** June 12-14; SPE Heavy Oil Conference Canada.
[13] A. M. Shehata, A. Ghatas, M. Kamel, A. Aly and A. Hassan, "Overview of Polymer Flooding (EOR) in North Africa Fields - Elements of Designing a New Polymer/Surfactant Flood Offshore (Case Study)", **(2012)** February 20-22; North Africa Technical Conference and Exhibition.
[14] K. Mohan, "Alkaline Surfactant Flooding for Tight Carbonate Reservoirs", **(2009)** October 4-7; SPE Annual Technical Conference and Exhibition.
[15] F. Xu, X. Guo, W. Wang, N. Zhang, S. Jia and X. Wang, "State Key Laboratory of Oil and Gas Reservoir Geology and Exploitation. Case Study: Numerical Simulation Of Surfactant Flooding In Low Permeability Oil Filed", **(2011)** July 19-21; SPE Enhanced Oil Recovery Conference.

Authors

Yin Daiyin

He received his PhD in Oil and Gas Field Development Engineer from Daqing Petroleum Institute, China in 2001. He received his bachelor degree in Reservoir Engineering and master degree in Oil and Gas Field Development Engineer from Daqing Petroleum Institute, China in 1988 and 1993 respectively. And he was a Post-Doc of Institute of Mechanics, Chinese Academy of Sciences. Currently, he is a professor in Department of Oil and Gas Field Development Engineer in Northeast Petroleum University, China. His research interests include reservoir geological modeling, numerical simulation and dynamic analysis on the development of oilfield.

Zhou Yazhou

He received the master's degree in Oil and Gas Field Development from Northeast Petroleum University, China in 2009, and received the bachelor's degree in Petroleum Engineering from Daqing Petroleum Institute, China in 2005. Currently, he is a PhD Candidate in Oil and Gas Engineering at Northeast Petroleum University. His research interests include reservoir numerical simulation, theory and technology of oil and gas field development.